



# External loops at the ferredoxin-NADP<sup>+</sup> reductase protein–partner binding cavity contribute to substrates allocation

Ana Sánchez-Azqueta<sup>a,b</sup>, Marta Martínez-Júlvez<sup>a,b</sup>, Manuel Hervás<sup>c</sup>, José A. Navarro<sup>c</sup>, Milagros Medina<sup>a,b,\*</sup>

<sup>a</sup> Departamento de Bioquímica Biología Molecular y Celular, Facultad de Ciencias, Universidad de Zaragoza, Zaragoza, Spain

<sup>b</sup> Institute of Biocomputation Physics of Complex Systems (BIFI)-Joint Unit BIFI-IQFR (CSIC), Universidad de Zaragoza, Zaragoza, Spain

<sup>c</sup> Instituto de Bioquímica Vegetal y Fotosíntesis, cicCartuja, Universidad de Sevilla & CSIC, Sevilla, Spain

## ARTICLE INFO

### Article history:

Received 21 October 2013

Received in revised form 20 November 2013

Accepted 27 November 2013

Available online 7 December 2013

### Keywords:

Ferredoxin-NADP<sup>+</sup> reductase

Electron and hydride transfer

Isoalloxazine:nicotinamide interaction

Catalytically competent interaction

Charge-transfer complex

## ABSTRACT

Ferredoxin-NADP<sup>+</sup> reductase (FNR) is the structural prototype of a family of FAD-containing reductases that catalyze electron transfer between low potential proteins and NAD(P)<sup>+</sup>/H, and that display a two-domain arrangement with an open cavity at their interface. The inner part of this cavity accommodates the reacting atoms during catalysis. Loops at its edge are highly conserved among plastidic FNRs, suggesting that they might contribute to both flavin stabilization and competent disposition of substrates. Here we pay attention to two of these loops in *Anabaena* FNR. The first is a sheet–loop–sheet motif, loop<sub>102–114</sub>, that allocates the FAD adenosine. It was thought to determine the extended FAD conformation, and, indirectly, to modulate isoalloxazine electronic properties, partners binding, catalytic efficiency and even coenzyme specificity. The second, loop<sub>261–269</sub>, contains key residues for the allocation of partners and coenzyme, including two glutamates, Glu267 and Glu268, proposed as candidates to facilitate the key displacement of the C-terminal tyrosine (Tyr303) from its stacking against the isoalloxazine ring during the catalytic cycle. Our data indicate that the main function of loop<sub>102–114</sub> is to provide the inter-domain cavity with flexibility to accommodate protein partners and to guide the coenzyme to the catalytic site, while the extended conformation of FAD must be induced by other protein determinants. Glu267 and Glu268 appear to assist the conformational changes that occur in the loop<sub>261–269</sub> during productive coenzyme binding, but their contribution to Tyr303 displacement is minor than expected. Additionally, loop<sub>261–269</sub> appears a determinant to ensure reversibility in photosynthetic FNRs.

© 2013 Elsevier B.V. All rights reserved.

## 1. Introduction

Ferredoxin-NADP<sup>+</sup> reductases (FNR) from photosynthetic organisms catalyze the production of NADPH in plants and cyanobacteria [1–3]. Their mechanisms are well characterized and they are the structural prototype for a large family of flavin-dependent oxido-reductases that participate in several biological reactions such as nitrogen fixation, steroid metabolism, iron–sulfur cluster biogenesis and oxidative-stress response [4,5]. Nevertheless, recent studies have indicated that additional residues to those directly implicated in the catalytic event,

might also have an important contribution at the molecular level to the enzyme functionality [3,6–10]. Members of the family share the presence of a basic module consisting on a flavin-binding domain (FAD or FMN) and a pyridine nucleotide-binding domain (NAD(P)<sup>+</sup>/H) [11]. Generally, the cavity at the interface between the two domains contains the electron carrier protein partner (ferredoxin (Fd) or flavodoxin (Fld)) binding site. Affinity and stability of the FNR complexes with its partners are mainly defined by direct contacts through their binding regions, but structural views indicate that more distant protein regions might also contribute to the overall process (Figure SM1) [3,12,13].

Structural comparison of some FNR-like representatives indicates differences in the conformation of their FAD cofactors (Fig. 1A). In plastidic-type FNRs the FAD is held in an L-shaped extended conformation, where the PPi group acts as a hinge and the adenosine moiety is bound to a flexible sheet–loop–sheet motif (loop<sub>102–114</sub> in *Anabaena* FNR (AnFNR)) where particular interactions are produced among the adenosine of FAD and the Tyr104 side-chain (including  $\pi$ – $\pi$  stacking and a H-bond between the adenosine O4 atom and the Tyr104 hydroxyl) [14–16]. In NAD-dependent proteins of the same structural family, such as nitrate reductases (NR) or cytochrome *b*<sub>5</sub> reductases (Cb5R), as well as in FNRs from proteobacteria, FAD shows different folded conformations [17–20]: for example, in rat Cb5R (rCb5R) the adenosine folds back, and sandwiched between a Tyr and a Phe

**Abbreviations:** FNR, ferredoxin-NADP<sup>+</sup> reductase; FNR<sub>ox</sub>, FNR in the fully oxidized state; FNR<sub>sq</sub>, FNR in the partially reduced state; FNR<sub>hq</sub>, FNR in the anionic hydroquinone (fully reduced) state; Fd, ferredoxin; Fd<sub>rd</sub>, ferredoxin in the reduced state; dRF, 5-deazariboflavin; ET, electron transfer; HT, hydride transfer; WT, wild-type; CTC, charge-transfer complex; NMN, nicotinamide nucleotide moiety of NADP<sup>+</sup>/H; 2'-P-AMP, 2'-P-AMP moiety of NADP<sup>+</sup>/H; PPi, pyrophosphate; *k*<sub>2</sub>, second-order rate constant; *k*<sub>obs</sub>, observed pseudo first-order rate constant; *k*<sub>1</sub> and *k*<sub>-1</sub>, association and dissociation rate constants, respectively, for complex formation; *I*, ionic strength; *k*<sub>HT</sub>, *k*<sub>HT-1</sub>, hydride transfer first-order rate constants for the forward and reverse reactions, respectively; *k*<sub>et</sub>, electron transfer rate constant

\* Corresponding author at: Departamento de Bioquímica y Biología Molecular y Celular, Facultad de Ciencias, Universidad de Zaragoza, E-50009 Zaragoza, Spain. Tel.: +34 976 762476; fax: +34 976 762123.

E-mail address: [mmolina@unizar.es](mailto:mmolina@unizar.es) (M. Medina).

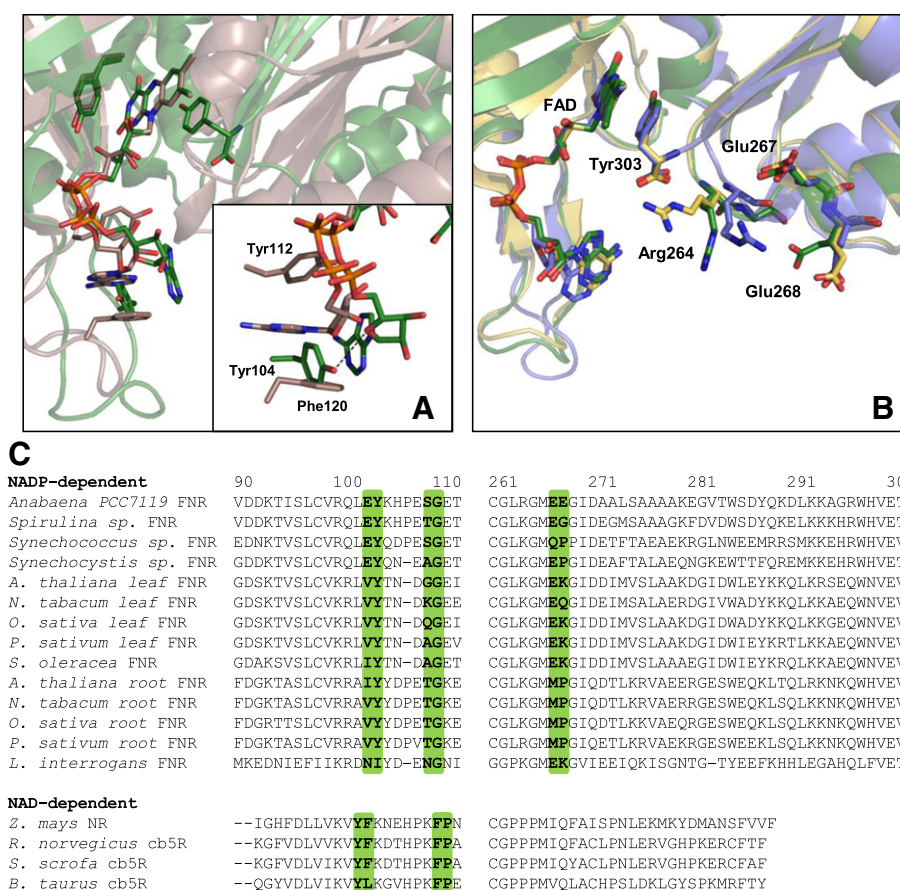


**Fig. 1.** Conformation of the FAD cofactor in the FNR family. (A) Superposition of crystal structures of AnFNR (PDB ID: 1QUE, in green) and rat Cb5R (PDB ID: 1I7P, in purple). Residues stacking the isoalloxazine and adenosine rings of FAD are shown as sticks. The inset shows a detail of the environment of the FAD adenosine moiety, stacked between Tyr112 and Phe120 in rat Cb5R and connected through H-bond and stacking interactions with Tyr104 in AnFNR. (B) Conformations of Arg264 and Glu268 in AnFNR (PDB ID: 1QUE, in green), in a NADP<sup>+</sup> complex (PDB ID: 1GJR (known as C-II), in blue) and in Y303F AnFNR (PDB ID: 2X3U, in yellow). (C) Sequence alignment of different NADP- and NAD-dependent members of the FNR superfamily (ClustalW2). Positions analyzed in this work are highlighted in green and numbers on the top correspond to the AnFNR numbering.

(Fig. 1A and C). Moreover, the catalytic efficiencies of bacterial FNR homologues and of NAD-dependent reductases, as well as their midpoint reduction potentials, differ from those of plastidic FNRs, inferring some relationship between these properties and the flavin conformation.

Electron (ET) and hydride (HT) transfer steps involving FNR<sub>hq/ox</sub> and NADP<sup>+</sup>/H or Fd<sub>ox/rd</sub>/Fd<sub>sq/hq</sub> are in general very fast processes, in which the enzyme specifically recognizes its partners and brings the reacting atoms into an optimal geometry [3,12,21–25]. During HT between FNR<sub>hq/ox</sub> and NADP<sup>+</sup>/H, the specific recognition of the phosphorylated pyridine nucleotide is guaranteed by the presence of a bipartite binding site in the enzyme that maintains the binding cavity inaccessible for the reactive nicotinamide nucleotide portion of NADP<sup>+</sup>/H (NMN) until accommodating its 2'-P-AMP moiety [26,27]. On the contrary, in NAD-dependent members of the family, the NAD-binding region consists of a preformed cavity able to accommodate the whole nucleotide without any protein re-arrangement [19,28–30]. Replacements in the 2'-P-AMP and P<sub>i</sub> binding regions of several FNRs have only provided minor improvements in modulating coenzyme specificity, with the only exception of the FNR from *Plasmodium falciparum* [31–35]. However, improvements in affinity for NAD<sup>+</sup>/H were reported when remodeling the NADP<sup>+</sup>/H binding cavity to create a preformed site, but these complexes were unproductive since the NMN moiety did not reach the active site [33]. This last step of the competent placement of the NMN moiety against the isoalloxazine relies on the displacement of the C-terminal tyrosine side-chain (Tyr303 in AnFNR). The exact forces and mechanism driving that movement still remain unknown [7,36–38],

but crystallographic data and molecular dynamic (MD) simulations pointed to a possible regulatory role played by Arg264. Its guanidinium has been detected adopting two main conformations: one interacting with the carboxylates of Glu267 and Glu268, and the other one connecting the Tyr303 terminal carboxylate (Fig. 1B and see Fig. 4 from [39]) [14,22,39].

In the present work, we gain further information about the particular roles of the above mentioned regions. Guided by sequence and structure alignments, we produced and characterized a single mutant, Y104F, and a multiple mutant, E103Y/Y104F/S109F/G110P, in loop<sub>102–114</sub> of AnFNR with the aim to mimic an environment that would induce a folded FAD conformation. On the other hand, the E267A/E268M AnFNR double mutant was conceived to prevent interactions of these residues with Arg264 during the catalytic event. The binding and catalytic properties of the three AnFNR variants, as well as their abilities for ET and HT, respectively, with Fd and NAD(P)<sup>+</sup>/H, are here reported, giving further clues about their roles in substrate recognition and NMN competent entrance into the active site.

## 2. Materials and methods

### 2.1. Biological material

The pET28a:AnFNR plasmids containing the Y104F, E103Y/Y104F/S109F/G110P and E267A/E268M mutations were obtained from the company Mutagenex® and used to produce the corresponding proteins from *Escherichia* cultures, which were purified as previously reported

[32]. *Anabaena* Fd (AnFd) was produced as previously described [24]. Protein samples were dialyzed in 50 mM Tris/HCl, pH 8.0 and concentrated using Amicon Ultra-15® centrifugal filters with a 10000 Da or a 5000 Da pore size for FNR or Fd, respectively. Protein preparations were made anaerobic by successive cycles of air evacuation and flushing with O<sub>2</sub>-free Ar in 50 mM Tris/HCl, pH 8.0. FNR<sub>hq</sub> variants were obtained by anaerobic photoreduction of the samples in the presence of 2 μM 5-deazariboflavin (dRf) and 3 mM EDTA in 50 mM Tris/HCl, pH 8.0 by irradiation from a 250 W light source [23].

## 2.2. Spectroscopic assays

UV–vis spectra were recorded in a Cary-100 spectrophotometer. The molar absorption coefficient for each FNR variant was spectrophotometrically determined by thermal denaturation of the protein for 10 min at 90 °C, followed by centrifugation and separation of the precipitated apoprotein, and spectroscopic quantification of the FAD released to the supernatant [40]. Photoreduction and potentiometric titrations were attempted in the presence of dRf/EDTA as previously reported [24]. These are long-lasting measurements where protein samples are illuminated and let under agitation at 25 °C, therefore, the low stability of the FNR mutants studied here prevented their full characterization. Interaction parameters with NADP<sup>+</sup> and NAD<sup>+</sup> were determined by difference absorption spectroscopy at 25 °C in 50 mM Tris/HCl, pH 8.0 as previously described [31]. Errors for the  $K_d$  and  $\Delta\epsilon$  values were  $\pm 10\%$  and  $\pm 5\%$ , respectively.

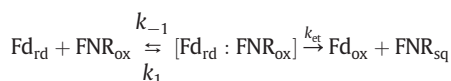
## 2.3. Steady-state kinetics measurements

The diaphorase activity of the FNR mutants was assayed in a double beam Cary-100 spectrophotometer using 2,6-dichlorophenolindophenol (DCPIP) ( $\Delta\epsilon_{620\text{nm}} 21 \text{ mM}^{-1}\text{cm}^{-1}$ ) or K<sub>3</sub>Fe(CN)<sub>6</sub> ( $\Delta\epsilon_{420\text{nm}} 1.05 \text{ mM}^{-1}\text{cm}^{-1}$ ) as two- or one-electron acceptors, respectively, and NADPH or NADH as electron donors. All measurements were carried out in 50 mM Tris/HCl, pH 8.0 at 25 °C. The final reaction mixture contained 4 nM FNR, either 0.1 mM DCPIP or 1.5 mM K<sub>3</sub>Fe(CN)<sub>6</sub>, and NADPH in the range 0–200 μM, or 1 μM FNR and higher nucleotide concentrations (0–5 mM) when assayed with NADH, while the reference cuvette contained 0.06 mM DCPIP when using this acceptor. The NADPH-dependent cytochrome *c* (Cyt<sub>c</sub>) reductase activity was determined using recombinant AnFd, and horse heart Cyt<sub>c</sub> as final electron acceptor. Reaction mixtures contained 4 nM FNR, 200 μM NADPH, 0.75 mg/ml Cyt<sub>c</sub> and 0–15 μM AnFd. Kinetic results were analyzed using a Michaelis–Menten model, and  $K_m$  and  $k_{\text{cat}}$  values were obtained by fitting the dependence of the observed initial rates on coenzyme concentration to this equation. Estimated errors in  $K_m$  and  $k_{\text{cat}}$  were  $\pm 10\%$  and  $\pm 5\%$ , respectively, for the diaphorase measurements, and  $\pm 20\%$  for the Cyt<sub>c</sub> activity.

## 2.4. Laser-flash induced kinetics

Time resolved ET reactions from AnFd<sub>rd</sub> to WT and E103Y/Y104F/S109F/G110P FNR<sub>ox</sub> were measured using laser-flash photolysis at 25 °C under anaerobic conditions in a 1 cm path-length cuvette, using EDTA as electron donor and dRf as photosensitizer, as previously described [41]. The standard reaction mixture contained, in a final volume of 1.5 mL, 4 mM sodium phosphate, pH 7.0, 1 mM EDTA and 100 μM dRf, in the presence (standard buffer) or the absence (low ionic strength (*I*) buffer) of 100 mM NaCl. Direct reduction of AnFNR<sub>ox</sub> by the laser-flash generated dRf semiquinone (dRfH•) was followed by measuring the decrease of absorbance at 458 nm. When both Fd in excess (40 μM) and FNR are present simultaneously in the solution, the subsequent ET process from the generated Fd<sub>rd</sub> to FNR<sub>ox</sub> can be monitored as the increase of absorbance at 600 nm due to the production of FNR<sub>sq</sub> [10,13,23,24]. Control experiments collected at 489–500 nm, an isosbestic point of the FNR<sub>ox</sub>/sq couple, allowed monitoring the

oxidation of Fd<sub>rd</sub>, yielding rate constants that were the same, within experimental error, as those determined from the 600 nm data. The effect of the ionic strength in the reaction was analyzed by adding aliquots of a 5 M NaCl solution to a reaction cuvette containing 40 μM AnFd and 30 μM AnFNR in low *I* buffer. All experiments were performed under pseudo-first-order conditions, for which the amount of acceptor (FNR<sub>ox</sub>) was maintained well in excess over the amount of the generated Fd<sub>rd</sub> (<1 μM). Each kinetic trace was the average of 8–15 measurements. All kinetic traces were fitted to monoexponential curves by using the Marquadt method to obtain the pseudo-first observed rate constants ( $k_{\text{obs}}$ ). Non-linear  $k_{\text{obs}}$  dependences on FNR concentration were adjusted to a two-step mechanism [23,42],



to estimate minimal values of both the forward association ( $k_1$ ) and reverse dissociation ( $k_{-1}$ ) rate constants, as well as the equilibrium dissociation constant ( $K_d = k_{-1}/k_1$ ) and the ET rate constant ( $k_{\text{et}}$ ). Errors in the estimated values of  $K_d$  and  $k_{\text{et}}$  were  $\pm 20\%$  and  $\pm 10\%$ , respectively.

## 2.5. Stopped-flow pre-steady-state kinetic measurements

Fast HT processes between the FNR<sub>hq/ox</sub> variants and NADP<sup>+</sup>/H, as well as between E267A/E268M FNR<sub>hq/ox</sub> and NAD<sup>+</sup>/H were followed by stopped-flow using an Applied Photophysics SX17.MV equipment with a photodiode array detector. Measurements were carried out in 50 mM Tris/HCl, pH 8.0 at 6 °C under anaerobic conditions as previously described [8,21]. Final FNR concentrations were 25 μM, while a 25–250 μM range was used for the nucleotide. Absorption spectra (400–1000 nm) were collected every 2.5 ms and processed using the X-Scan software (App. Photo. Ltd.). Analysis of time dependent spectral changes was performed by global analysis and numerical integration methods using Pro-Kineticist (App. Photo. Ltd.). The observed conversion rate constants ( $k_{A \rightarrow B}$ ,  $k_{B \rightarrow C}$ ) were calculated by fitting the collected data to a single step model. In most cases, a previous reaction ( $A \rightarrow B$ ) had occurred within the instrumental death time, leading to charge transfer complex (CTC) formation. In those cases we correlate the measurable reaction to a  $B \rightarrow C$  model, being B and C spectral species reflecting a distribution of enzyme intermediates (reactants, CTCs, products, Michaelis complexes) at a certain point along the reaction time course, and not necessarily a single distinct enzyme intermediate. Model validity was assessed by the lack of systematic deviations from residual plots at different wavelengths, inspection of calculated spectra and consistence among the number of significant singular values with the fitting model. In general, no dependence profiles on the NADP<sup>+</sup>/H concentration were observed for the HT processes analyzed, probably due to the reversibility of the processes and the maximal  $k_{B \rightarrow C}$  values were obtained at the 1:1. Since it was not possible to determine reduction midpoint potentials for the mutants analyzed here we were not able to globally fit the apparent rate constants as a function of coenzyme concentration to the sum of the rates for the forward ( $k_{\text{HT}}$ ) and reverse ( $k_{\text{HT}-1}$ ) HT at equilibrium [22,43]. Therefore, as accepted in similar cases [8,21], we related  $k_{B \rightarrow C}$  with the maximal experimental HT rate constant,  $k_{\text{HT}}$  or  $k_{\text{HT}-1}$ , values. For the reduction of E267A/E268M FNR,  $k_{A \rightarrow B}$  derived from experimental data showed a dependence profile on the NADPH concentration fitting to the equation describing binding at a single site followed by the HT process,

$$k_{A \rightarrow B} = \frac{k_{\text{HT}-1}(K_d + [\text{NADPH}]) + k_{\text{HT}}[\text{NADPH}]}{[\text{NADPH}] + K_d}$$

and allowed the determination of  $K_d$  and  $k_{\text{HT}}$  values. Errors in the estimated values of  $K_d$  and  $k_{\text{HT}}$  values were  $\pm 20\%$  and  $\pm 15\%$ , respectively, while those of  $k_{A \rightarrow B}$  or  $k_{B \rightarrow C}$  were  $\pm 10\%$ .



## 2.6. Crystal growth, data collection and structure refinement

The E103Y/Y104F/S109F/G110P variant of AnFNR was crystallized under same conditions as those reported for WT FNR [27]. X-ray dataset was collected in the ID23-1 line at ESRF (Grenoble, France) and processed with XDS [44] and SCALA from CCP4 [45]. The first model was obtained by MOLREP [46] from CCP4, using the WT FNR structure (1QUE) as template. Refinement of the structure was performed with Refmac5 [47] from CCP4, alternating with manual model building with COOT [48]. PROCHECK [49] and MOLPROBITY [50] programs were used to assess final structure. A single crystal of E103Y/Y104F/S109F/G110P FNR diffracted up to 1.70 Å and belonged to the  $P6_5$  hexagonal space group. Its  $V_m$  was 2.95 Å<sup>3</sup>/Da with one FNR molecule in the asymmetric unit and 58.4% solvent content. The model comprised residues 9–303, one FAD molecule, one  $SO_4^{2-}$  ion, one glycerol molecule and water molecules. Data for collection and refinement processes can be found in Table SP1. The coordinates and structure factors for this FNR variant have been deposited with PDB ID: 4C43.

## 3. Results

### 3.1. Spectral properties of the FNR<sub>ox</sub> variants and interaction with the coenzyme

The level of expression in *E. coli* of all the FNR mutants was similar to that of WT, and purification yielded well-folded and FAD assembled FNRs. The mutants showed similar spectral properties to WT AnFNR<sub>ox</sub>, with absorbance maxima of the flavin band-I at 458 nm and extinction coefficients at this wavelength not varying significantly, indicating no major structural perturbations in the close environment of the FAD isoalloxazine ring. However, Y104F FNR suffered some loss of the FAD cofactor when dialyzed, and E267A/E268M FNR was not soluble at concentrations over 60 μM. Moreover, stepwise photoreduction of Y104F, E103Y/Y104F/S109F/G110P and E267A/E268M FNRs induced FAD dissociation and protein denaturation, preventing determination of their midpoint reduction potentials. These observations indicate that the mutations particularly affect the strength of the ApoFNR:FAD<sub>hq</sub> complex, suggesting weakening of the affinity for the reduced form of the cofactor.

Difference spectra obtained upon titration of Y104F, E103Y/Y104F/S109F/G110P and E267A/E268M FNRs with NADP<sup>+</sup> were similar to those for the WT protein, with only minor displacements of the positions of minima and maxima (Fig. 2). The hyperbolic dependence of the absorbance changes upon increasing NADP<sup>+</sup> concentrations allowed determination of  $K_d^{NADP^+}$  as well as of the magnitude of the

change upon complex formation,  $\Delta\epsilon$  (Table 1).  $K_d^{NADP^+}$  did not vary significantly either being just slightly smaller, 1.5-fold for the Y104F and E103Y/Y104F/S109F/G110P FNRs, or up to 3.3-fold for E267A/E268M FNR. Therefore while the loop<sub>102–114</sub> appears to have minor effects on NADP<sup>+</sup> binding, the glutamates in positions 267 and/or 268 in the WT enzyme appear contributing to reduce the affinity for this form of the coenzyme. Titration of all FNR variants with NAD<sup>+</sup> did not induce any difference spectra, indicating that this coenzyme was not able to produce changes in the flavin environment. This suggests that its nicotinamide ring is not bound in the enzyme flavin environment.

### 3.2. Steady-state kinetic parameters of the FNR mutants

Either DCPIP or potassium ferricyanide, as final artificial two- or one-electron acceptors respectively, were used to obtain the diaphorase steady-state kinetic parameters of the FNR variants (Table 1). Y104F and E103Y/Y104F/S109F/G110P FNRs displayed behaviors very similar to that of WT, though in general  $k_{cat}$  values slightly decreased. Regarding E267A/E268M FNR,  $k_{cat}$  values were also slightly lower and  $K_m^{NADPH}$  values were within 2-fold of those of the WT: increasing when using ferricyanide as electron acceptor and decreasing when using DPCIP. Therefore, the E267A/E268M FNR catalytic efficiency increased around 2-fold when using a two-electron acceptor, while decreased in a similar range when using a one-electron acceptor. Finally, the diaphorase activity of E267A/E268M FNR showed a remarkable  $k_{cat}$  increase regarding WT FNR when using NADH as electron donor. As consequence, this variant was two orders of magnitude less specific for NADPH versus NADH than the WT.

The introduced mutations produced more important deleterious effects in the Fd mediated NADPH dependent Cyt<sub>c</sub> reductase activity of FNR (Table 2). Despite E103Y/Y104F/S109F/G110P FNR exhibited a similar behavior to the WT in terms of  $k_{cat}$ , this parameter resulted reduced by 8- and 2.5-fold for Y104F and E267A/E268M FNRs, respectively. Moreover,  $K_m^{Fd}$  increased for all the variants, but particularly for those at loop<sub>102–114</sub>, suggesting that the mutations reduce the affinity of FNR for Fd, at least in an optimal orientation for ET. All together these parameters indicate that the introduced mutations, but particularly the single replacement of Tyr104 by Phe, have an important negative impact in the non-photosynthetic ET from FNR to Fd.

### 3.3. Transient kinetics for ET from Fd to FNR

The low stability of Y104F and E267A/E268M FNRs prevented their characterization by laser-flash spectroscopy. However, direct reduction of the E103Y/Y104F/S109F/G110P FNR isoalloxazine to its neutral semiquinone form by the laser-flash generated dRfH• could be followed by a decrease of the absorption at 458 nm following a monoexponential decay, as observed for the WT FNR [23].  $k_{obs}$  values resulted linearly dependent on the FNR concentration and allowed obtaining second-order bimolecular rate constants ( $k_2$ ) of the same order of magnitude as for the WT (Table 3) [23]. This observation indicated that this mutant is as efficiently reduced by dRfH• as WT.

In the presence of an excess of Fd<sub>ox</sub>, the laser-generated dRfH• causes the initial fast reduction of this protein, followed by a subsequent ET step from Fd<sub>rd</sub> to FNR<sub>ox</sub>, that can be monitored by an absorption increase at 600 nm due to formation of the neutral FNR<sub>sq</sub> [23,24]. Reduction of FNR<sub>ox</sub> by Fd<sub>rd</sub> has been investigated here in the presence of a moderately high salt concentration ( $I = 120$  mM), conditions reported as optimal for this ET reaction [23]. Moreover,  $k_{obs}$  values presented a hyperbolic dependence on enzyme concentration that can be related with the formation of a transient FNR<sub>ox</sub>:Fd<sub>rd</sub> complex prior to the ET step (Fig. 3A) [51]. The two-step model here applied to estimate  $K_d$  and  $k_{et}$  values has largely demonstrated to be useful in the characterization of ET in transient protein:protein reactions [10,13,41,42,52]. The model is based in the total amount of FNR<sub>ox</sub> in the sample as it is widely accepted that, in transient protein complexes, protein association/

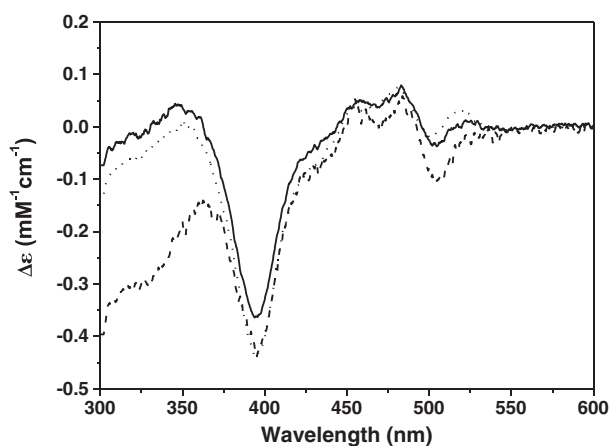


**Fig. 2.** Interaction of the FNR mutants with the coenzyme. Difference absorbance spectra elicited upon titration of WT (—), E103Y/Y104F/S109F/G110P (·····) and E267A/E268M (---) FNRs (~20 μM) with saturating concentrations of NADP<sup>+</sup> in 50 mM Tris/HCl, pH 8.0 and 25 °C.

**Table 1**

Steady-state kinetic parameters of the different FNR<sub>ox</sub> variants for the interaction with NADP<sup>+</sup> and for the diaphorase activity. Measurements were carried out in 50 mM Tris/HCl, pH 8.0 at 25 °C.

FNR variant	Interaction parameters		Diaphorase steady-state kinetic parameters								
	DCPIP										
	NADP <sup>+</sup>		NADPH			NADH			Fe(CN) <sub>6</sub> <sup>3-</sup>		
	$K_d^{\text{NADP}^+}$ (μM)	$\Delta\epsilon_{(482-390)}$ (mM <sup>-1</sup> cm <sup>-1</sup> )	$K_m$ (μM)	$k_{\text{cat}}$ (s <sup>-1</sup> )	$k_{\text{cat}}/K_m$ (μM <sup>-1</sup> s <sup>-1</sup> )	$K_m$ (μM)	$k_{\text{cat}}$ (s <sup>-1</sup> )	$k_{\text{cat}}/K_m$ (μM <sup>-1</sup> s <sup>-1</sup> )	$K_m$ (μM)	$k_{\text{cat}}$ (s <sup>-1</sup> )	$k_{\text{cat}}/K_m$ (μM <sup>-1</sup> s <sup>-1</sup> )
WT <sup>a</sup>	4.0	1.15	6.0	81.5	13.6	800	0.16	$2.0 \times 10^{-4}$	11	370	34
Y104F	2.7	1.34 <sup>b</sup>	6.4	84.2	13.2	665	0.35	$5.3 \times 10^{-4}$	16	265	16.6
E103Y/Y104F/S109F/G110P	2.8	1.35 <sup>c</sup>	4.7	67.3	14.3	651	0.27	$4.1 \times 10^{-4}$	14	257	18.4
E267A/E268M	1.2	1.15 <sup>d</sup>	2.7	67.6	25.0	518	14	$2.7 \times 10^{-2}$	22	309	14

<sup>a</sup> Data from [10].

<sup>b</sup> Using  $\Delta\epsilon_{(484-395)}$ .

<sup>c</sup> Using  $\Delta\epsilon_{(481-394)}$ .

<sup>d</sup> Using  $\Delta\epsilon_{(485-396)}$ .

dissociation is much faster than ET itself, and thus the ET process would be the rate limiting step rather than protein exchange. Thus, applying the formalism previously described [42], minimal values for  $k_{\text{et}}$ ,  $k_1$  and  $k_{-1}$  (and  $K_d$ ) could be estimated (Table 3). These values suggested a slight (2-fold) increase in the affinity of the Fd:FNR complex induced by the introduced mutations, whereas the ET process remains basically unaffected.

The influence of  $I$  was further analyzed to investigate the effects induced by the combined E103Y/Y104F/S109F/G110P mutations on the Fd:FNR interaction. As reported for the WT, biphasic dependences of  $k_{\text{obs}}$  with increasing  $I$  were also observed for the variant (Fig. 3B). The bell-shaped profile for the dependence of  $k_{\text{obs}}$  with  $I$  is related with the re-arrangement of the initial FNR<sub>ox</sub>:Fd<sub>rd</sub> encounter transient complex to achieve an optimal ET conformation, indicating the occurrence of protein–protein dynamic motions that are blocked by strong electrostatic interactions at very low  $I$  [23]. However, the  $k_{\text{obs}}$  maximum was shifted to higher  $I$  for the mutant, suggesting the occurrence of stronger electrostatic interactions in the encounter complex than in the WT system.

### 3.4. Transient kinetics of the hydride transfer reactions

Fast HT processes between WT AnFNR<sub>hq/ox</sub> and NADP<sup>+</sup>/H occur through the formation of two intermediate CTCs [21,22]: [FNR<sub>ox</sub>–NADPH] (CTC-1, characterized by an absorbance spectral band with maximum at ~600 nm), and [FNR<sub>hq</sub>–NADP<sup>+</sup>] (CTC-2, showing a broad band centered at ~800 nm). The HT event occurs in the transition of CTC-1 to CTC-2, or *vice versa*. Similarly to the WT, reduction of Y104F, E103Y/Y104F/S109F/G110P and E267A/E268M AnFNR<sub>ox</sub>s by NADPH showed CTC-1 formation and protein reduction (measured by the decrease of the flavin band-I absorbance at 458 nm) in the instrumental dead time, with subsequent spectral evolution including additional reduction of the enzyme and formation of CTC-2 (Fig. 4A–D). This multiple wavelength spectral evolution best fitted to a single-step model that includes the HT event, and thus the observed rate constants are named  $k_{B \rightarrow C}$ . For the Y104F and E103Y/

**Table 2**

Steady-state kinetic parameters of the different FNR<sub>ox</sub> variants in the NADPH-dependent cytochrome c reductase activity. Measurements in 50 mM Tris/HCl, pH 8.0 at 25 °C.

FNR variant	$K_m^{\text{Fd}}$ (μM)	$k_{\text{cat}}$ (s <sup>-1</sup> )	$k_{\text{cat}}/K_m$ (μM <sup>-1</sup> s <sup>-1</sup> )
WT <sup>a</sup>	1.0	176	176
Y104F	5.7	22.2	4
E103Y/Y104F/S109F/G110P	6.1	166.7	27
E267A/E268M	2.1	66.7	31.7

<sup>a</sup> Data from [10].

Y104F/S109F/G110P variants,  $k_{B \rightarrow C}$  values were independent on the NADPH concentration as in the WT, being, therefore, related with limiting  $k_{\text{HT}}$  values (Table 4). However, a concentration dependence hyperbolic profile was observed for the E267A/E268M FNR process allowing the determination of a  $K_d^{\text{NADPH}}$  value that suggested a weaker FNR: NADPH interaction than in WT (Table 4). Nevertheless, significant negative effects on  $k_{\text{HT}}$  were not observed in any of the mutants.

Y104F and E103Y/Y104F/S109F/G110P FNRs also behaved very similar to WT AnFNR when assaying the reverse reaction. Thus, reduction of NADP<sup>+</sup> by these FNR<sub>hq</sub> variants showed appearance of a small amount of CTC-2 concomitant with mild protein reoxidation within the instrumental dead time, followed by subsequent spectral evolution including flavin oxidation and CTC-1 formation (Fig. 4E–G). Kinetic parameters for these processes were also similar to those of WT (Table 4). On the contrary, HT from E267A/E268M FNR<sub>hq</sub> to NADP<sup>+</sup> occurred with minor CTC stabilization (Fig. 4H), particularly of CTC-2, and with a 2-fold decrease in  $k_{\text{HT-1}}$ .

HT processes for E267A/E268M FNR were also assayed with the non-phosphorylated pyridine nucleotide, NAD<sup>+</sup>/H, to determine if the augmented steady-state catalytic efficiency observed for this variant with NADH might be a consequence of a more efficient HT reaction. Similarly to that reported for the WT, reactions between E267A/E268M FNR and NAD<sup>+</sup>/H were extremely slow processes that did not lead to CTC stabilization (not shown) [33]. Nevertheless, comparison of rate constants for WT and E267A/E268M FNRs using a 1:5 protein:NAD<sup>+</sup>/H ratio, led to a slight increase in the apparent HT rate constants by the introduced mutations ( $k_{A \rightarrow B}^{\text{WT}} = 0.02 \text{ s}^{-1}$  and  $k_{A \rightarrow B}^{\text{E267A/E268M}} = 0.08 \text{ s}^{-1}$  for the reduction by NADH and  $k_{A \rightarrow B}^{\text{WT}} = 0.1 \text{ s}^{-1}$  and  $k_{A \rightarrow B}^{\text{E267A/E268M}} = 0.8 \text{ s}^{-1}$  for oxidation by NAD<sup>+</sup>).

### 3.5. The structural environment of the mutated positions

The overall folding of E103Y/Y104F/S109F/G110P AnFNR is pretty similar to that of WT AnFNR (0.73 Å for 295Cα atoms aligned). Poor

**Table 3**

Parameters for the laser-flash induced reduction of the different FNR variants by dRfH• and AnFd<sub>rd</sub>.

FNR variant	Reduction by dRfH• <sup>a</sup>	Reduction by AnFd <sub>rd</sub> <sup>b</sup>			
	$k_2$ (M <sup>-1</sup> s <sup>-1</sup> )	$k_1$ (μM <sup>-1</sup> s <sup>-1</sup> )	$k_{-1}$ (s <sup>-1</sup> )	$k_{\text{et}}$ (s <sup>-1</sup> )	$K_d$ (μM)
WT	$2.3 \times 10^8$	$5.2 \times 10^2$	$9.0 \times 10^3$	$7.8 \times 10^3$	17.0
E103Y/Y104F/ S109F/G110P	$3.8 \times 10^8$	$1.0 \times 10^3$	$7.5 \times 10^3$	$6.4 \times 10^3$	7.5

<sup>a</sup> In 4 mM phosphate, pH 7.0 ( $I = 20 \text{ mM}$ ).

<sup>b</sup> In 4 mM phosphate, pH 7.0, and 100 mM NaCl ( $I = 120 \text{ mM}$ ).

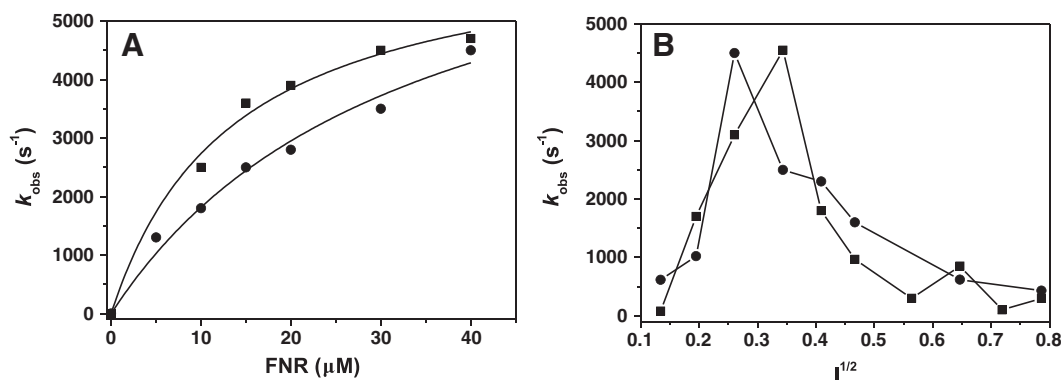


**Fig. 3.** Transient ET from  $\text{Fd}_{\text{rd}}$  to E103Y/Y104F/S109F/G110P  $\text{FNR}_{\text{ox}}$ . (A) Dependence on  $\text{FNR}_{\text{ox}}$  concentration of the observed rate constants ( $k_{\text{obs}}$ ) for the reduction by  $\text{Fd}_{\text{rd}}$  of WT (●) and E103Y/Y104F/S109F/G110P (■) FNR at  $I = 120 \text{ mM}$ . Reaction mixtures contained  $40 \mu\text{M}$   $\text{Fd}_{\text{ox}}$ . (B) Dependence on the square root of  $I$  of  $k_{\text{obs}}$  for the reduction of WT (●) and E103Y/Y104F/S109F/G110P (■)  $\text{FNR}_{\text{ox}}$  by  $\text{Fd}_{\text{rd}}$ . Samples contained  $30 \mu\text{M}$   $\text{FNR}_{\text{ox}}$  and  $40 \mu\text{M}$   $\text{Fd}_{\text{ox}}$ . Reactions were carried out in 4 mM phosphate, pH 7.0 and  $25^\circ\text{C}$ .

electron density did not allow determining the position of residues 106 and 107. However residues flanking them, including the mutated ones, show a good density that allows describing the peptide chain in this region. Mutations on the adenosine binding loop did not lead to a remarkable change in the overall positioning of FAD that keeps extended conformation with only its adenosine moiety differing somehow in conformation regarding to the WT structure (Fig. 5). The absence of the Tyr104 hydroxyl, in the WT FNR H-bonding the ribose O4 atom (Fig. 5B), is compensated by an intramolecular H-bond between both adenosine O4 and N3 atoms that seems to force a twist and a slight displacement of the adenosine moiety (Fig. 5C). On the other hand and due to the introduced mutations, the loop shows a more open conformation than in the WT structure. So, in the mutant the loop<sub>102–114</sub> points outwards and differs from its WT conformation with an r.m.s.d. of 4.18 Å. Another significant structural feature observed in the mutant structure concerns to the conformation of the Arg264 side-chain (Fig. 5). As already described in other AnFNR structures [10,22], its guanidinium group moves, in this mutant 5 Å, towards the Tyr303 carboxylate. This observation reinforces the idea of differently populated orientations of this Arg side-chain in position during coenzyme binding and catalysis.

## 4. Discussion

### 4.1. The sheet–loop–sheet motif (loop<sub>102–114</sub> in AnFNR) binding the FAD adenosine in plastidic FNRs

The comparison of plastidic FNRs with NAD-dependent members of the family (Fig. 1A and C) drove us to the production of two variants in the FAD adenosine binding loop<sub>102–114</sub>: Y104F and E103Y/Y104F/S109F/G110P FNRs. The Y104F mutant was intended to disrupt the H-bond between the Tyr104-OH and the FAD adenosine, while keeping the stacking interaction with the aromatic side-chain. On the other hand, the E103Y/Y104F/S109F/G110P one was expected to induce a change in the orientation of loop<sub>102–114</sub> towards that displayed by some NADH-dependent members of the family (Fig. 1A). However, the crystal structure of E103Y/Y104F/S109F/G110P FNR resulted practically identical to that of the WT protein, with the FAD in an extended conformation very similar to the WT enzyme (Fig. 5). Moreover, the inherent flexibility of loop<sub>102–114</sub> and of the FAD adenosine moiety in plastidic FNRs [27,39] is even enhanced in the mutant. This might counteract changes in the shape of the flavin binding site introduced by the mutations. Similarly, an unaltered FAD conformation has been observed in two engineered pea and *E. coli* FNRs (plastidic- and bacterial-type FNRs, respectively) upon deletion and insertion, respectively, of the plastidic characteristic adenosine binding strand–loop–strand motif [53]. Therefore, the binding and kinetic effects induced by these mutations in AnFNR must account mainly for changes in the nature of their side-chains rather than to the expected alterations on FAD conformation. In AnFNR, most of

the protein connections with the ribose and adenine moieties of FAD are bridged by water molecules, and only one direct H-bond is established with Tyr104-OH. Disruption of this connection in the Y104F mutant appears to have an important impact in FAD affinity, particularly in its reduced state. However, the lack of stability of this variant was recovered upon introduction of the three additional mutations in E103Y/Y104F/S109F/G110P FNR, where, although the WT contact between the FAD and the loop was still missing, a new FAD intramolecular H-bond between both adenosine O4 and N3 atoms forces a twist in the adenine orientation and the displacement of this adenosine moiety (Fig. 5).

Apart from weaker FAD binding, substitutions in the loop<sub>102–114</sub> did not lead to major changes on FNR overall folding, nor in its  $\text{NAD(P)}^+/\text{H}$  binding and catalytic parameters (Tables 1 and 4). Nevertheless, some effects were particularly observed in the affinity for the protein partner, with minor effects on ET rates ( $k_{\text{et}}$  and  $k_{\text{cat}}$ ) (Tables 1, 2 and 3). This might be related with the clear retraction observed in the position of the loop<sub>102–114</sub> upon the introduction of the mutations regarding those in free WT FNR and in the Fd:FNR samples, which appears having a negative effect in the initial recognition event between partners (Figure SM2). All together these data suggest that the main function of the loop<sub>102–114</sub> is to provide flexibility to the inter-domain cavity to assist the guiding of the coenzyme and, particularly, of the protein partners and to their binding cavities, while other structural determinants will be responsible for the FAD extended conformation.

### 4.2. Role of loop<sub>261–269</sub> in AnFNR in the competent binding of substrates

The simultaneous substitutions of Glu267 and Glu268 in AnFNR also affected the affinity for the protein partner (Table 1). The crystal structure of the AnFd:AnFNR complex situates Arg264 and Glu267 at the complex interface, H-bonding Fd-Tyr25/Arg42, and Asp62, respectively (Figure SM3) [13,25,54]. E267A/E268M FNR eliminates two negative charges on the FNR surface, as well as the possibility of H-bonding at position 267, and, conceivably the displacement of the native Arg264 arrangement might be possible. Therefore, both the initial interaction governed by electrostatic attractive forces and the subsequent optimal complex surface adjustment would be affected, thus explaining the increase on  $K_{\text{d}}^{\text{Fd}}$  and the decrease on  $k_{\text{cat}}$  observed for the CytC reductase activity (Table 2), and also in agreement with previously reported deleterious effects for the D62K AnFd mutant [55]. Additionally, the midpoint reduction potential appears altered in the mutant, making ET to Fd less favorable. Binding and HT data for E267A/E268M FNR with the coenzyme are indicative of higher  $\text{FNR}_{\text{ox}}:\text{NADP}^+$  and lower  $\text{FNR}_{\text{ox}}:\text{NADPH}$  affinities, but with final catalytic geometries optimal and non-optimal for  $\text{FNR}_{\text{ox}}:\text{NADPH}$  and  $\text{FNR}_{\text{red}}:\text{NADP}^+$ , respectively (Tables 1 and 4). Therefore, a role must be accepted for these two residues in coenzyme accommodation during catalysis, and in ensuring that the

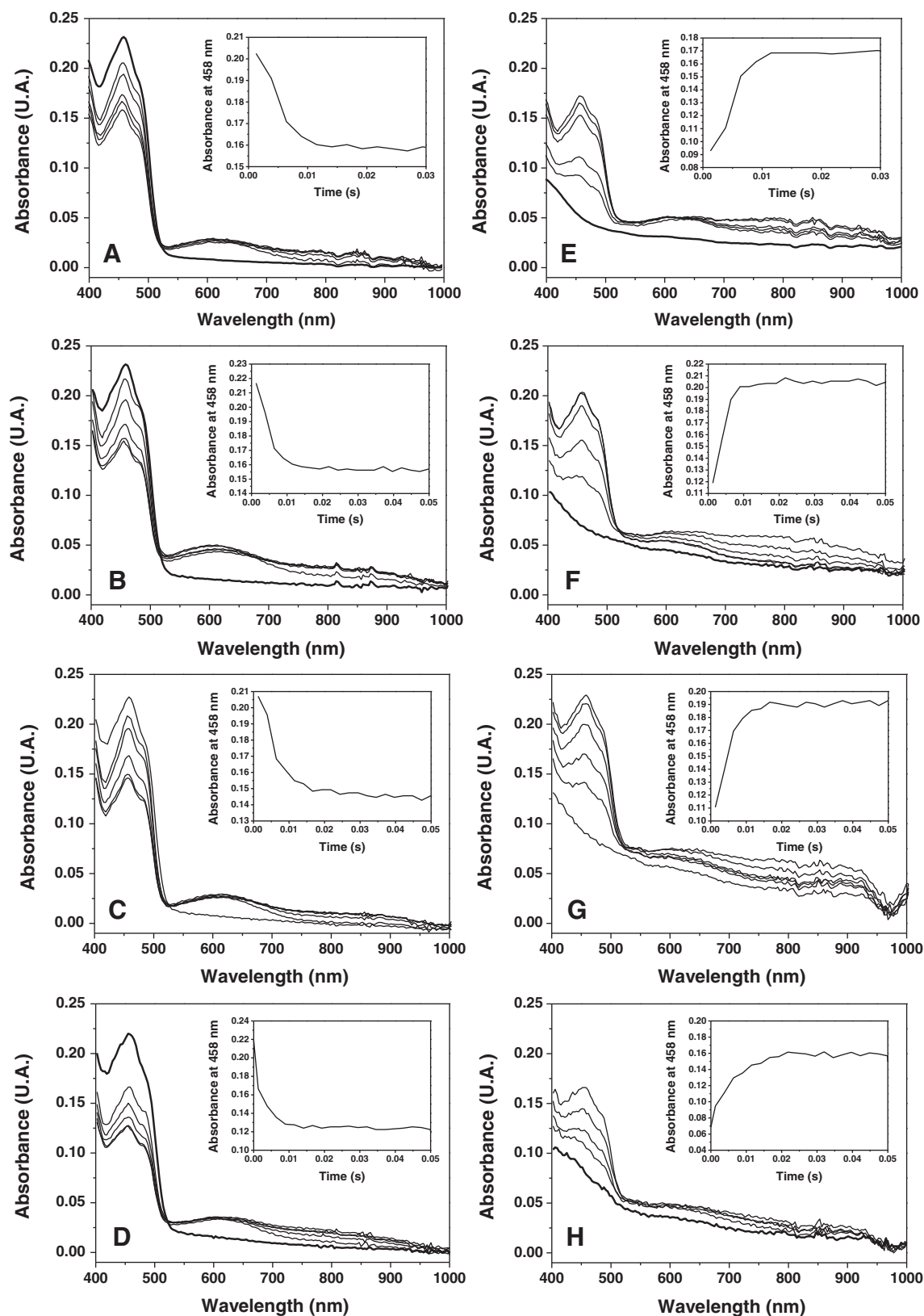


**Fig. 4.** Transient HT processes between the FNR variants and the coenzyme. Evolution of the spectral changes observed during the HT reactions of different FNR<sub>ox/hq</sub> mutants (25  $\mu$ M) with NADP<sup>+</sup>/H (100  $\mu$ M) in 50 mM Tris/HCl, pH 8.0 at 6 °C. Reduction of (A) WT, (B) Y104F, (C) E103Y/Y104F/S109F/G110P and (D) E267A/E268M FNR<sub>ox</sub> with NADPH and oxidation of (E) WT, (F) Y104F, (G) E103Y/Y104F/S109F/G110P and (H) E267A/E268M FNR<sub>hq</sub> with NADP<sup>+</sup>. In all cases spectra were recorded at 0.00128 s, 0.00384 s, 0.0064 s, 0.0192 s and 0.2547 s; the thick line is the spectrum of the oxidized/reduced protein before reacting and the inset shows the time evolution of the absorbance at 458 nm.

reaction is able to take place either in the photosynthetic or non-photosynthetic directions as required by the organism, a particular feature of plastidic FNRs. This is in agreement with loop<sub>261–269</sub> being a

determinant for competent NADP<sup>+</sup>/H recognition and NMN allocation [8,32,33]. Thus, loop<sub>261–269</sub> undergoes several conformational changes during the proposed three-step (WT  $\rightarrow$  C-I  $\rightarrow$  C-II  $\rightarrow$  C-III) NADP<sup>+</sup>/H



**Table 4**

Transient-kinetics parameters for the HT and HT-1 processes between the different FNR<sub>hq/ox</sub> and NADP<sup>+</sup>/H. Measured in 50 mM Tris/HCl, pH 8.0 at 6 °C.

FNR variant	FNR <sub>ox</sub> and NADPH		FNR <sub>hq</sub> and NADP <sup>+</sup>	
	$K_d^{\text{NADPH}}$ ( $\mu\text{M}^{-1}$ )	$k_{\text{HT1}}$ ( $\text{s}^{-1}$ )	$K_d^{\text{NADP}^+}$ ( $\mu\text{M}^{-1}$ )	$k_{\text{HT-1}}$ ( $\text{s}^{-1}$ )
WT	–	270	–	290
Y104F	–	277	–	281
E103Y/Y104F/S109F/G110P	–	247	–	287
E267A/E268M	18.6	290	–	133

binding process [27], which involve changes in the conformation of Arg264 and Glu267 side-chains and in the interactions they establish along the transitions (Fig. 6A). In WT and C-I, the C-terminal Tyr303 carboxylate and the Thr302-OH are situated at H-bond distance of the Arg264 amide and the Glu267 carboxylate, respectively. The transition of C-I into C-II (Fig. 6A to Fig. 6B) entails displacement of loop<sub>261–269</sub> and rotation of the Leu263 side-chain to accommodate the PPi and NMN moieties, breaking Arg264-Tyr303 and Glu267-Thr302 H-bonds. Finally, allocation of the NMN moiety into the active site in C-III (represented by the structure of the Y303S FNR:NADP<sup>+</sup> complex) appears accompanied by partial return of loop<sub>261–269</sub> to its original position (Fig. 6C). Thus, the C-ter-loop<sub>261–269</sub> connections must first break apart to allow Leu263 displacement, and then get restored to assist Tyr303 displacement; two steps crucial for competent coenzyme binding. The low E267A/E268M FNR stability prevented its crystallization, but we constructed its structural model. This model suggested a displacement of loop<sub>261–269</sub> with respect to the original template structure, and resembled that of the C-II complex (Fig. 6B), reinforcing the proposed influence of a Glu267-Thr302 bond in positioning of loop<sub>261–269</sub> regarding Tyr303. This conformation can explain both the higher E267A/E268M FNR<sub>ox</sub>:NADP<sup>+</sup> affinity and the enhanced NADH activity due to the fact that the nucleotide entrance is less blocked by the side-chain of

Leu263, thus making 2'-P-AMP recognition less critical for optimal co-enzyme binding (Table 1). Displacement of Tyr303 is hence proposed as a consequence of additive forces that all together compensate for the disruption of  $\pi$ - $\pi$  stacking and H-bond interactions with Ser80 and Glu301: the nicotinamide ring pushes Tyr303 from one side while the loop<sub>261–269</sub> pulls from the other. Additional concerted roles played by other protein regions are not discarded. Among them, the movement of Glu301 and the loss of its H-bond connection with Tyr303-OH [56] and the assistance by Fd binding [57,58] may be especially relevant. According to E267A/E268M FNR  $k_{\text{HT}}$  and  $k_{\text{HT-1}}$  values (Table 4), contribution of loop<sub>261–269</sub> to Tyr303 displacement appears to be more important in the photosynthetic HT reaction, while the pushing effect of the nicotinamide would dominate the backward process. MD simulations further support this hypothesis [39]. Similarly, the HT reaction from a FNR<sub>hq</sub> mutant previously produced at Arg264, R264E, to NADP<sup>+</sup> slightly slowed down compared to WT, while  $k_{\text{HT}}$  values remained unaltered [25]. The different effects observed depending on the HT direction might be also related to divergences in the sequences of the loop<sub>261–269</sub> among plant-type reductases (Fig. 1C). Glu267 is conserved among photosynthetic FNRs and the presence of a glutamate in the following position is characteristic of some cyanobacterial enzymes, while higher plants have a Lys and a non-polar side-chain is found in the position equivalent to Thr302. The characteristic Glu-Lys pair of leaf FNRs is replaced by a Met-Pro one in FNRs from plant roots and other non-photosynthetic organisms, such as *Leptospira interrogans* FNR. This, together with observed differences in residues at positions equivalent to loop<sub>261–269</sub> and NMN occupancy upon NADP<sup>+</sup> binding may be related to the preferential direction of their physiologically catalyzed reactions [11,15,59–61]. Thus, loop<sub>261–269</sub> might contain the determinants for the reversibility of the HT process in photosynthetic FNRs.

In conclusion, the AnFNR mutants here analyzed on the FAD adenosine and NADP<sup>+</sup> binding loops further confirm the complexity of the mechanisms addressing oxido-reduction partner selectivity and

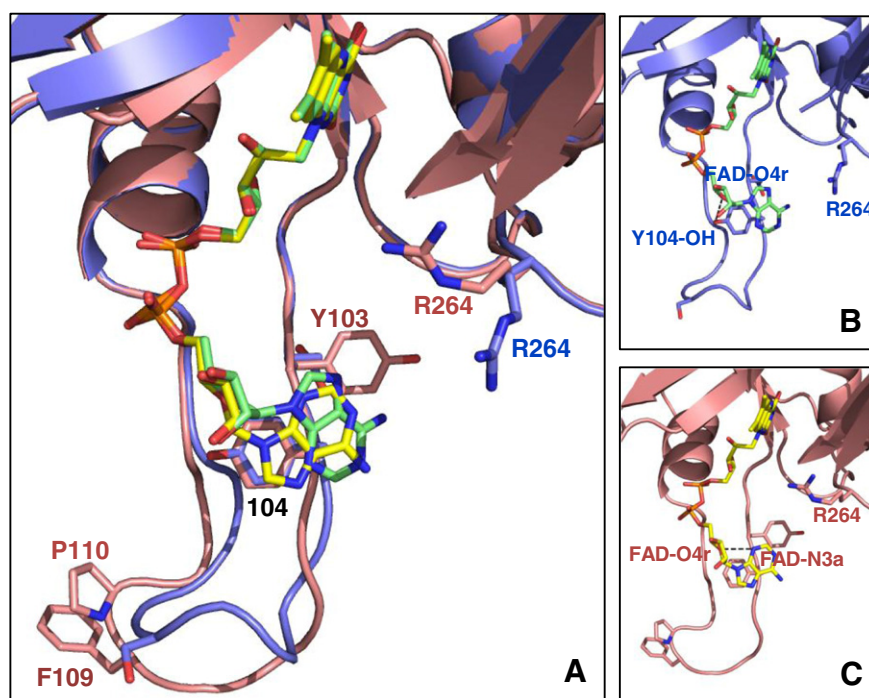


**Fig. 5.** Crystal structure of E103Y/Y104F/S109F/G110P FNR. (A) Comparison of the three-dimensional structures of WT (blue, FAD in green) and E103Y/Y104F/S109F/G110P (pink, FAD in yellow) AnFNRs in the FAD environment. Detail of the H-bond between the ribose O4 atom in (B) WT and (C) E103Y/Y104F/S109F/G110P AnFNRs. FAD and mutated side-chains are represented in CPK colored sticks.



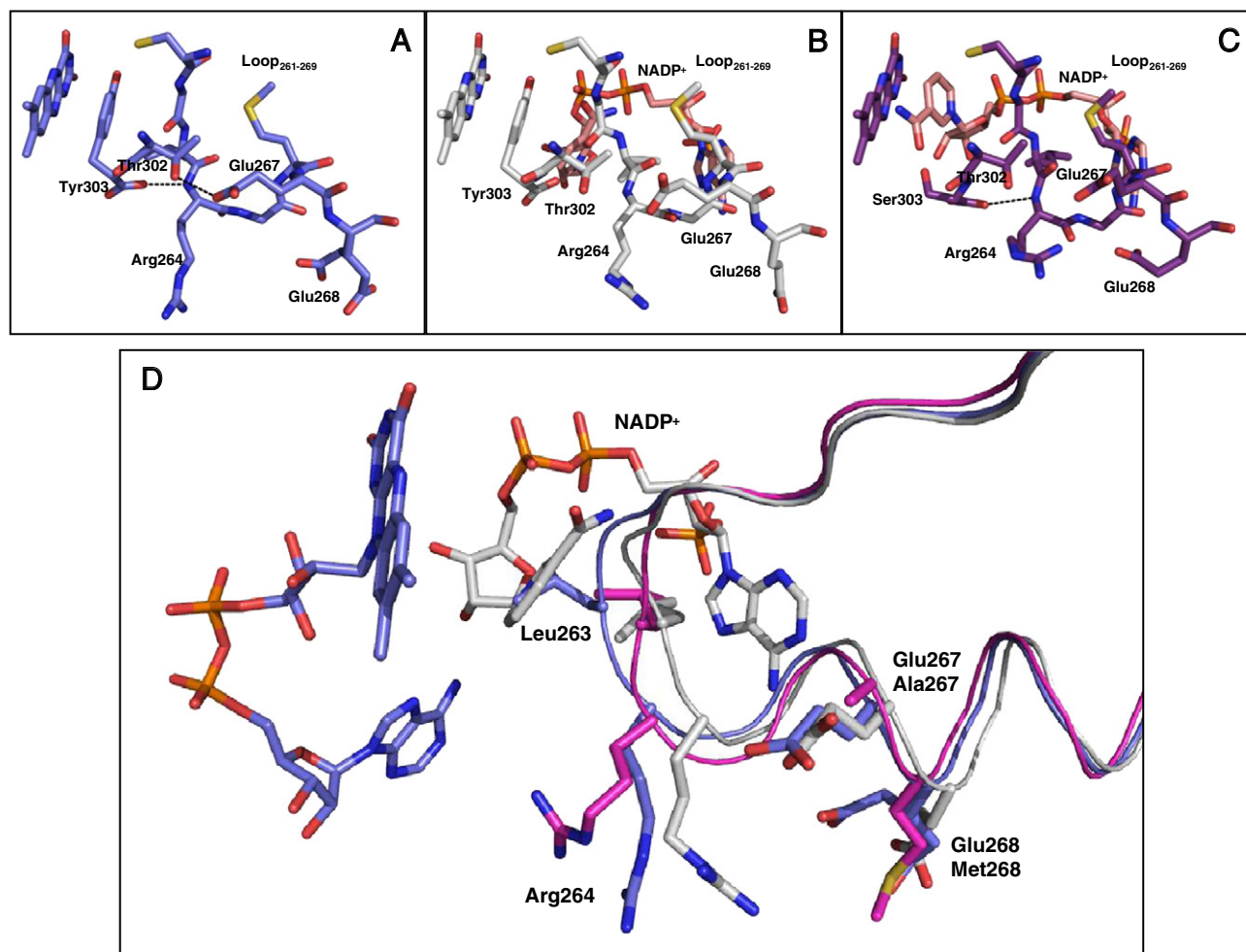


**Fig. 6.** Conformation of the FNR loop<sub>261–269</sub> along catalysis. Conformations of loop<sub>261–269</sub> and some of its key residues in (A) WT AnFNR (PDB 1QUE, blue), and in (B) C-II (PDB 1GJR, gray) and (C) C-III (PDB 2BSA, purple) complexes with NADP<sup>+</sup> (pink pale sticks). The Thr302–Glu267 and Tyr303–Arg264 interactions are shown as dashed lines. (D) Superposition in the loop<sub>261–269</sub> region of the structure theoretically predicted for E267A/E268M FNR (pink), WT AnFNR (PDB 1QUE, blue) and C-II FNR:NADP<sup>+</sup> complex (PDB 1GJR, gray). Side-chains for positions 263, 264, 267 and 268 are represented as CPK sticks. The E267A/E268M FNR theoretical model was produced using the Geno3D server [62] and AnFNR WT (PDB 1QUE) as template.

catalytic efficiency in these reductases, in agreement with previous unsuccessful attempts to re-design FNRs with modified binding and/or HT properties. The results here presented conclude that the flexibility of loop<sub>102–114</sub> allows a competent final relative distance of the redox catalytic centers, particularly modulating Fd binding and ET. Additionally, direct interactions between the side-chain of Arg264 and those of Glu267 and Glu268 do not play a crucial role in Tyr303 displacement. Nevertheless, all they participate in the NADP<sup>+</sup>/H binding processes assisting the conformational changes that occur in the loop<sub>261–269</sub> during productive coenzyme binding as well as to the reversibility of the HT process.

### Acknowledgements

This work has been supported by MINECO, Spain (Grant BIO2010-14983 to M.M) and the Andalusian Government-FEDER (PAIDI BIO-022 to J.A.N.). A. S-A holds a FPU fellowship from the Spanish Ministry of Education.

### Appendix A. Supplementary data

Supplementary data to this article can be found online at <http://dx.doi.org/10.1016/j.bbabbio.2013.11.016>.

### References

- [1] A.K. Arakaki, E.A. Ceccarelli, N. Carrillo, Plant-type ferredoxin-NADP<sup>+</sup> reductases: a basal structural framework and a multiplicity of functions, *FASEB J.* 11 (1997) 133–140.
- [2] E.A. Ceccarelli, A.K. Arakaki, N. Cortez, N. Carrillo, Functional plasticity and catalytic efficiency in plant and bacterial ferredoxin-NADP(H) reductases, *Biochim. Biophys. Acta* 1698 (2004) 155–165.
- [3] M. Medina, Structural and mechanistic aspects of flavoproteins: photosynthetic electron transfer from photosystem I to NADP<sup>+</sup>, *FEBS J.* 276 (2009) 3942–3958.
- [4] A. Aliverti, V. Pandini, A. Pennati, M. de Rosa, G. Zanetti, Structural and functional diversity of ferredoxin-NADP<sup>+</sup> reductases, *Arch. Biochem. Biophys.* 474 (2008) 283–291.
- [5] P.A. Karplus, C.M. Bruns, Structure–function relations for ferredoxin reductase, *J. Bioenerg. Biomembr.* 26 (1994) 89–99.
- [6] N. Carrillo, E.A. Ceccarelli, Open questions in ferredoxin-NADP<sup>+</sup> reductase catalytic mechanism, *Eur. J. Biochem.* 270 (2003) 1900–1915.
- [7] I. Lans, M. Medina, E. Rosta, G. Hummer, M. García-Viloca, J.M. Lluch, A. González-Lafont, Theoretical study of the mechanism of the hydride transfer between ferredoxin-NADP<sup>+</sup> reductase and NADP<sup>+</sup>: the Role of Tyr303, *J. Am. Chem. Soc.* 134 (2012) 20544–20553.
- [8] A. Sánchez-Azqueta, M.A. Musumeci, M. Martínez-Júlvez, E.A. Ceccarelli, M. Medina, Structural backgrounds for the formation of a catalytically competent complex with NADP(H) during hydride transfer in ferredoxin-NADP<sup>+</sup> reductases, *Biochim. Biophys. Acta* 1817 (2012) 1063–1071.
- [9] A. Bortolotti, A. Sánchez-Azqueta, C.M. Maya, A. Velázquez-Campoy, J.A. Hermoso, M. Medina, N. Cortez, The C-terminal extension of bacterial flavodoxin-reductases: Involvement in the hydride transfer mechanism from the coenzyme, *Biochim. Biophys. Acta* 2014 (1837) 33–43.
- [10] A. Sánchez-Azqueta, B. Herguedas, R. Hurtado-Guerrero, M. Hervás, J.A. Navarro, M. Martínez-Júlvez, M. Medina, A hydrogen bond network in the active site of *Anabaena* ferredoxin-NADP<sup>+</sup> reductase modulates its catalytic efficiency, *Biochim. Biophys. Acta* (2013), <http://dx.doi.org/10.1016/j.bbabbio.2013.10.010>.

- [11] P.A. Karplus, M.J. Daniels, J.R. Herriott, Atomic structure of ferredoxin-NADP<sup>+</sup> reductase: prototype for a structurally novel flavoenzyme family, *Science* 251 (1991) 60–66.
- [12] M. Medina, C. Gómez-Moreno, Interaction of ferredoxin-NADP<sup>+</sup> reductase with its substrates: optimal interaction for efficient electron transfer, *Photosynth. Res.* 79 (2004) 113–131.
- [13] J.K. Hurley, R. Morales, M. Martínez-Júlviz, T.B. Brodie, M. Medina, C. Gómez-Moreno, G. Tollin, Structure–function relationships in *Anabaena* ferredoxin/ferredoxin-NADP<sup>+</sup> reductase electron transfer: insights from site-directed mutagenesis, transient absorption spectroscopy and X-ray crystallography, *Biochim. Biophys. Acta* 1554 (2002) 5–21.
- [14] L. Serre, F.M. Vellieux, M. Medina, C. Gómez-Moreno, J.C. Fontecilla-Camps, M. Frey, X-ray structure of the ferredoxin:NADP<sup>+</sup> reductase from the cyanobacterium *Anabaena* PCC 7119 at 1.8 Å resolution, and crystallographic studies of NADP<sup>+</sup> binding at 2.25 Å resolution, *J. Mol. Biol.* 263 (1996) 20–39.
- [15] Z. Deng, A. Aliverti, G. Zanetti, A.K. Arakaki, J. Ottado, E.G. Orellano, N.B. Calcaterra, E.A. Ceccarelli, N. Carrillo, P.A. Karplus, A productive NADP<sup>+</sup> binding mode of ferredoxin-NADP<sup>+</sup> reductase revealed by protein engineering and crystallographic studies, *Nat. Struct. Biol.* 6 (1999) 847–853.
- [16] C.M. Bruns, P.A. Karplus, Refined crystal structure of spinach ferredoxin reductase at 1.7 Å resolution: oxidized, reduced and 2'-phospho-5'-AMP bound states, *J. Mol. Biol.* 247 (1995) 125–145.
- [17] I. Nogués, I. Pérez-Dorado, S. Frago, C. Bittel, S.G. Mayhew, C. Gómez-Moreno, J.A. Hermoso, M. Medina, N. Cortez, N. Carrillo, The ferredoxin-NADP(H) reductase from *Rhodobacter capsulatus*: molecular structure and catalytic mechanism, *Biochemistry* 44 (2005) 11730–11740.
- [18] M. Ingelman, S. Ramaswamy, V. Niviere, M. Fontecave, H. Eklund, Crystal structure of NAD(P)H: flavin oxidoreductase from *Escherichia coli*, *Biochemistry* 38 (1999) 7040–7049.
- [19] G. Lu, Y. Lindqvist, G. Schneider, U. Dwivedi, W. Campbell, Structural studies on corn nitrate reductase: refined structure of the cytochrome *b* reductase fragment at 2.5 Å, its ADP complex and an active-site mutant and modeling of the cytochrome *b* domain, *J. Mol. Biol.* 248 (1995) 931–948.
- [20] M.C. Bewley, C.C. Marohnic, M.J. Barber, The structure and biochemistry of NADH-dependent cytochrome *b*<sub>5</sub> reductase are now consistent, *Biochemistry* 40 (2001) 13574–13582.
- [21] J. Tejero, J.R. Peregrina, M. Martínez-Júlviz, A. Gutiérrez, C. Gómez-Moreno, N.S. Scrutton, M. Medina, Catalytic mechanism of hydride transfer between NADP<sup>+</sup>/H and ferredoxin-NADP<sup>+</sup> reductase from *Anabaena* PCC 7119, *Arch. Biochem. Biophys.* 459 (2007) 79–90.
- [22] J.R. Peregrina, A. Sánchez-Azqueta, B. Herguedas, M. Martínez-Júlviz, M. Medina, Role of specific residues in coenzyme binding, charge-transfer complex formation, and catalysis in *Anabaena* ferredoxin-NADP<sup>+</sup> reductase, *Biochim. Biophys. Acta* 1797 (2010) 1638–1646.
- [23] M. Medina, M. Martínez-Júlviz, J.K. Hurley, G. Tollin, C. Gómez-Moreno, Involvement of glutamic acid 301 in the catalytic mechanism of ferredoxin-NADP<sup>+</sup> reductase from *Anabaena* PCC 7119, *Biochemistry* 37 (1998) 2715–2728.
- [24] I. Nogués, J. Tejero, J.K. Hurley, D. Paladini, S. Frago, G. Tollin, S.G. Mayhew, C. Gómez-Moreno, E.A. Ceccarelli, N. Carrillo, M. Medina, Role of the C-terminal tyrosine of ferredoxin-nicotinamide adenine dinucleotide phosphate reductase in the electron transfer processes with its protein partners ferredoxin and flavodoxin, *Biochemistry* 43 (2004) 6127–6137.
- [25] M. Martínez-Júlviz, J. Hermoso, J.K. Hurley, T. Mayoral, J. Sanz-Aparicio, G. Tollin, C. Gómez-Moreno, M. Medina, Role of Arg100 and Arg264 from *Anabaena* PCC 7119 ferredoxin-NADP<sup>+</sup> reductase for optimal NADP<sup>+</sup> binding and electron transfer, *Biochemistry* 37 (1998) 17680–17691.
- [26] D.H. Paladini, M.A. Musumeci, N. Carrillo, E.A. Ceccarelli, Induced fit and equilibrium dynamics for high catalytic efficiency in ferredoxin-NADP(H) reductases, *Biochemistry* 48 (2009) 5760–5768.
- [27] J.A. Hermoso, T. Mayoral, M. Faro, C. Gomez-Moreno, J. Sanz-Aparicio, M. Medina, Mechanism of coenzyme recognition and binding revealed by crystal structure analysis of ferredoxin-NADP<sup>+</sup> reductase complexed with NADP<sup>+</sup>, *J. Mol. Biol.* 319 (2002) 1133–1142.
- [28] C.C. Correll, C.J. Batie, D.P. Ballou, M.L. Ludwig, Phthalate dioxygenase reductase: a modular structure for electron transfer from pyridine nucleotides to [2Fe–2S], *Science* 258 (1992) 1604–1610.
- [29] H. Nishida, K. Inaka, M. Yamanaka, S. Kaida, K. Kobayashi, K. Miki, Crystal structure of NADH-cytochrome *b*<sub>5</sub> reductase from pig liver at 2.4 Å resolution, *Biochemistry* 34 (1995) 2763–2767.
- [30] C.C. Marohnic, M.C. Bewley, M.J. Barber, Engineering and characterization of a NADPH-utilizing cytochrome *b*<sub>5</sub> reductase, *Biochemistry* 42 (2003) 11170–11182.
- [31] M. Medina, A. Luquita, J. Tejero, J. Hermoso, T. Mayoral, J. Sanz-Aparicio, K. Grever, C. Gómez-Moreno, Probing the determinants of coenzyme specificity in ferredoxin-NADP<sup>+</sup> reductase by site-directed mutagenesis, *J. Biol. Chem.* 276 (2001) 11902–11912.
- [32] J. Tejero, M. Martínez-Júlviz, T. Mayoral, A. Luquita, J. Sanz-Aparicio, J.A. Hermoso, J.K. Hurley, G. Tollin, C. Gómez-Moreno, M. Medina, Involvement of the pyrophosphate and the 2'-phosphate binding regions of ferredoxin-NADP<sup>+</sup> reductase in coenzyme specificity, *J. Biol. Chem.* 278 (2003) 49203–49214.
- [33] J.R. Peregrina, B. Herguedas, J.A. Hermoso, M. Martínez-Júlviz, M. Medina, Protein motifs involved in coenzyme interaction and enzymatic efficiency in *Anabaena* ferredoxin-NADP<sup>+</sup> reductase, *Biochemistry* 48 (2009) 3109–3119.
- [34] A. Aliverti, T. Lubberstedt, G. Zanetti, R.G. Herrmann, B. Curti, Probing the role of lysine 116 and lysine 244 in the spinach ferredoxin-NADP<sup>+</sup> reductase by site-directed mutagenesis, *J. Biol. Chem.* 266 (1991) 17760–17763.
- [35] S. Baroni, V. Pandini, M.A. Vanoni, A. Aliverti, A single tyrosine hydroxyl group almost entirely controls the NADPH specificity of *Plasmodium falciparum* ferredoxin-NADP<sup>+</sup> reductase, *Biochemistry* 51 (2012) 3819–3826.
- [36] L. Piubelli, A. Aliverti, A.K. Arakaki, N. Carrillo, E.A. Ceccarelli, P.A. Karplus, G. Zanetti, Competition between C-terminal tyrosine and nicotinamide modulates pyridine nucleotide affinity and specificity in plant ferredoxin-NADP<sup>+</sup> reductase, *J. Biol. Chem.* 275 (2000) 10472–10476.
- [37] J. Tejero, I. Pérez-Dorado, C. Maya, M. Martínez-Júlviz, J. Sanz-Aparicio, C. Gómez-Moreno, J.A. Hermoso, M. Medina, C-terminal tyrosine of ferredoxin-NADP<sup>+</sup> reductase in hydride transfer processes with NAD(P)<sup>+</sup>/H, *Biochemistry* 44 (2005) 13477–13490.
- [38] I. Lans, J.R. Peregrina, M. Medina, M. García-Viloca, A. González-Lafont, J.M. Lluch, Mechanism of the hydride transfer between *Anabaena* Tyr303Ser FNR<sub>rd</sub>/FNR<sub>ox</sub> and NADP<sup>+</sup>/H. A combined pre-steady-state kinetic/ensemble-averaged transition-state theory with multidimensional tunneling study, *J. Phys. Chem. B* 114 (2010) 3368–3379.
- [39] J.R. Peregrina, I. Lans, M. Medina, The transient catalytically competent coenzyme allocation into the active site of *Anabaena* ferredoxin-NADP<sup>+</sup> reductase, *Eur. Biophys. J.* 41 (2012) 117–128.
- [40] P. Macheroux, UV-visible spectroscopy as a tool to study flavoproteins, *Methods Mol. Biol.* 131 (1999) 1–7.
- [41] V. Rodríguez-Roldán, J.M. García-Heredia, J.A. Navarro, M. Hervás, B. De la Cerda, F.P. Molina-Heredia, M.A. De la Rosa, A comparative kinetic analysis of the reactivity of plant, horse, and human respiratory cytochrome *c* towards cytochrome *c* oxidase, *Biochem. Biophys. Res. Commun.* 346 (2006) 1108–1113.
- [42] T.E. Meyer, Z.G. Zhao, M.A. Cusanovich, G. Tollin, Transient kinetics of electron transfer from a variety of *c*-type cytochromes to plastocyanin, *Biochemistry* 32 (1993) 4552–4559.
- [43] S. Daff, An appraisal of multiple NADPH binding-site models proposed for cytochrome P450 reductase, NO synthase, and related diflavin reductase systems, *Biochemistry* 43 (2004) 3929–3932.
- [44] W. Kabsch, Automatic processing of rotation diffraction data from crystals of initially unknown symmetry and cell constants, *J. Appl. Crystallogr.* 26 (1993) 795–800.
- [45] M.D. Winn, C.C. Ballard, K.D. Cowtan, E.J. Dodson, P. Emsley, P.R. Evans, R.M. Keegan, E.B. Krissinel, A.G. Leslie, A. McCoy, S.J. McNicholas, G.N. Murshudov, N.S. Pannu, E.A. Potterton, H.R. Powell, R.J. Read, A. Vagin, K.S. Wilson, Overview of the CCP4 suite and current developments, *Acta Crystallogr. D Biol. Crystallogr.* 67 (2011) 235–242.
- [46] A. Vagin, A. Teplyakov, MOLREP: an automated program for molecular replacement, *J. Appl. Crystallogr.* 30 (1997) 1022–1025.
- [47] G.N. Murshudov, A.A. Vagin, E.J. Dodson, Refinement of macromolecular structures by the maximum-likelihood method, *Acta Crystallogr. D Biol. Crystallogr.* 53 (1997) 240–255.
- [48] P. Emsley, B. Lohkamp, W.G. Scott, K. Cowtan, Features and development of Coot, *Acta Crystallogr. D Biol. Crystallogr.* 66 (2010) 486–501.
- [49] R.A. Laskowski, M.W. MacArthur, D.S. Moss, J.M. Thornton, PROCHECK: a program to check the stereochemical quality of protein structures, *J. Appl. Crystallogr.* 26 (1993) 283–291.
- [50] I.W. Davis, A. Leaver-Fay, V.B. Chen, J.N. Block, G.J. Kapral, X. Wang, L.W. Murray, W.B. Arendall III, J. Snoeyink, J.S. Richardson, D.C. Richardson, MolProbity: all-atom contacts and structure validation for proteins and nucleic acids, *Nucleic Acids Res.* 35 (2007) W375–W383.
- [51] J.K. Hurley, J.L. Schmeits, C. Genzor, C. Gómez-Moreno, G. Tollin, Charge reversal mutations in a conserved acidic patch in *Anabaena* ferredoxin can attenuate or enhance electron transfer to ferredoxin:NADP<sup>+</sup> reductase by altering protein/protein orientation within the intermediate complex, *Arch. Biochem. Biophys.* 333 (1996) 243–250.
- [52] S. Frago, I. Lans, J.A. Navarro, M. Hervás, D.E. Edmondson, M.A. De la Rosa, C. Gómez-Moreno, S.G. Mayhew, M. Medina, Dual role of FMN in flavodoxin function: electron transfer cofactor and modulation of the protein–protein interaction surface, *Biochim. Biophys. Acta* 1797 (2010) 262–271.
- [53] M.A. Musumeci, H. Botti, A. Buschiazio, E.A. Ceccarelli, Swapping FAD binding motifs between plastidic and bacterial ferredoxin-NADP(H) reductases, *Biochemistry* 50 (2011) 2111–2122.
- [54] R. Morales, M.H. Charon, G. Kachalova, L. Serre, M. Medina, C. Gómez-Moreno, M. Frey, A redox-dependent interaction between two electron-transfer partners involved in photosynthesis, *EMBO Rep.* 1 (2000) 271–276.
- [55] J.K. Hurley, A.M. Weber-Main, M.T. Stankovich, M.M. Benning, J.B. Thoden, J.L. Vanhook, H.M. Holden, Y.K. Chae, B. Xia, H. Cheng, J.L. Markley, M. Martínez-Júlviz, C. Gómez-Moreno, J.L. Schmeits, G. Tollin, Structure–function relationships in *Anabaena* ferredoxin: correlations between X-ray crystal structures, reduction potentials, and rate constants of electron transfer to ferredoxin:NADP<sup>+</sup> reductase for site-specific ferredoxin mutants, *Biochemistry* 36 (1997) 11100–11117.
- [56] V.I. Dumit, T. Essigke, N. Cortez, G.M. Ullmann, Mechanistic insights into ferredoxin-NADP(H) reductase catalysis involving the conserved glutamate in the active site, *J. Mol. Biol.* 397 (2010) 814–825.
- [57] C.J. Batie, H. Kamin, Electron transfer by ferredoxin:NADP<sup>+</sup> reductase. Rapid-reaction evidence for participation of a ternary complex, *J. Biol. Chem.* 259 (1984) 11976–11985.
- [58] C.J. Batie, H. Kamin, Ferredoxin:NADP<sup>+</sup> oxidoreductase. Equilibria in binary and ternary complexes with NADP<sup>+</sup> and ferredoxin, *J. Biol. Chem.* 259 (1984) 8832–8839.
- [59] J. Sancho, C. Gómez-Moreno, Interaction of ferredoxin-NADP<sup>+</sup> reductase from *Anabaena* with its substrates, *Arch. Biochem. Biophys.* 288 (1991) 231–238.
- [60] A. Aliverti, R. Faber, C.M. Finnerty, C. Ferioli, F. Pandini, A. Negri, P.A. Karplus, G. Zanetti, Biochemical and crystallographic characterization of ferredoxin-NADP<sup>+</sup> reductase from nonphotosynthetic tissues, *Biochemistry* 40 (2001) 14501–14508.
- [61] Y. Onda, T. Matsumura, Y. Kimata-Arigo, H. Sakakibara, T. Sugiyama, T. Hase, Differential interaction of maize root ferredoxin:NADP<sup>+</sup> oxidoreductase with photosynthetic and non-photosynthetic ferredoxin isoproteins, *Plant Physiol.* 123 (2000) 1037–1045.
- [62] C. Combet, M. Jambon, G. Deléage, C. Geourjon, Geno3D: automatic comparative molecular modelling of protein, *Bioinform. Comput. Appl. Biosci.* 18 (2002) 213–214.